Title
Proton affinities of pertechnetate (TcO 4 −) and perrhenate (ReO 4 −)

Journal
Physical Chemistry Chemical Physics, 22(22)

ISSN
1463-9076

Authors
Jian, Jiwen
Varathan, Elumalai
Cheisson, Thibault
et al.

Publication Date
2020-06-10

DOI
10.1039/d0cp01721c

Peer reviewed

Proton affinities of pertechnetate (TcO_4^-) and perrhenate (ReO_4^-)†

Jiwen Jian,‡[a] Elumalai Varathan,[b] Thibault Cheisson,§[c] Tian Jian,[a] Wayne W. Lukens,[a] Rebecca L. Davis,[b] Eric J. Schelter,[c] Georg Schreckenbach*[b] and John K. Gibson*[a]

The anions pertechnetate, TcO_4^-, and perrhenate, ReO_4^-, exhibit very similar chemical and physical properties. Revealing and understanding disparities between them enhances fundamental understanding of both. Electrospray ionization generated the gas-phase proton bound dimer $(TcO_4^-)(H^+)(ReO_4^-)$. Collision induced dissociation of the dimer yielded predominantly $HTcO_4$ and ReO_4^-, which according to Cooks' kinetic method indicates that the proton affinity (PA) of TcO_4^- is greater than that of ReO_4^-. Density functional theory computations agree with the experimental observation, providing PA[TcO_4^-] = 300.1 kcal mol^{-1} and PA[ReO_4^-] = 297.2 kcal mol^{-1}. Attempts to rationalize these relative PAs based on elementary molecular parameters such as atomic charges indicate that the entirety of bond formation and concomitant bond disruption needs to be considered to understand the energies associated with such protonation processes. Although in both the gas and solution phases, TcO_4^- is a stronger base than ReO_4^-, it is noted that the significance of even such qualitative accordance is tempered by the very different natures of the underlying phenomena.

Introduction

Pertechnetate, TcO_4^-, and perrhenate, ReO_4^-, are tetrahedral anions that exhibit very similar chemistry. With the negative charge distributed among four oxygen atoms, these MO_4^- ions, like ClO_4^-,[1] exhibit "soft" coordination behavior that results in outer sphere complexation in solution and relatively modest hydration energies.[2] Extensive efforts aimed at selective removal of TcO_4^- from aqueous solution reflects the fact that it is the predominant and environmentally mobile form of radioactive ^{99}Tc, which is a prevalent and problematic nuclear fission product.[3] Separation of ReO_4^- from other anions has received less attention than TcO_4^-, but is nonetheless of interest given potential applications of beta-emitting ^{188}Re (16.9 h half-life) in nuclear medicine.[4] Pursuit of selective receptors for TcO_4^- and ReO_4^- generally has an ultimate goal of separation from other environmentally and industrially prevalent anions such as Cl^-, NO_3^- and SO_4^{2-}.[5–7] Less familiar, and generally less imperative from a practical perspective, is the much more challenging separation of TcO_4^- and ReO_4^- from one another. Successful separation of these two chemically similar species would advance their separations from other anions. In addition, widespread use of ReO_4^- containing stable naturally occurring isotopes of Re as a surrogate for radioactive $^{99}TcO_4^-$ motivates understanding differences between these two species.[8] Furthermore, as for other chemically similar elements in the same group of the periodic table, revealing fundamental differences between Tc and Re is key to better comprehending the chemistry of both.

The original objective of this work was to assess comparative affinities of TcO_4^- and ReO_4^- for an organic ligand that can readily form hydrogen bonds, namely the protonated tripodal nitroxide ligand $[(2\text{-}^t\text{BuNOH})C_6H_4CH_2]_3N$, denoted as H_3TriNOx and shown in Fig. 1.[9] H_3TriNOx presents three accessible hydroxyl moieties as potential H-bonding sites.[10] The strategy was to use electrospray ionization (ESI) to generate gas-phase complexes comprising TcO_4^- and/or ReO_4^- coordinated by H_3TriNOx. It was anticipated that relative abundances of different complexes would reveal differences in efficacy of anion coordination by the ligand, and that collision induced dissociation (CID)

[a] Chemical Sciences Division, Lawrence Berkeley National Laboratory, Berkeley, California, 94720, USA. E-mail: jkgibson@lbl.gov
[b] Department of Chemistry, University of Manitoba, Winnipeg, Manitoba, R3T 2N2, Canada. E-mail: schrecke@cc.umanitoba.ca
[c] Department of Chemistry, University of Pennsylvania, Philadelphia, Pennsylvania, 19104, USA

† Electronic supplementary information (ESI) available: Complete citations for ref. 18 and 19; bond distances, NBO bond orders, and NPA charges of species in reactions (1) and (2); frequencies for Tc–O and Re–O vibrational modes; PAs of TcO_4^- and ReO_4^- calculated with different functionals and basis sets; CID mass spectra of $[(L)(H^+)]$ and $(TcO_4^-)(H^+)(ReO_4^-)$; ESI mass spectrum of a L/TcO_4^-/ReO_4^- solution; structures and energies of $(L)[(TcO_4^-)(H^+)(ReO_4^-)]$. See DOI: 10.1039/d0cp01721c

‡ Present address: Hangzhou Institute of Advanced Studies, Zhejiang Normal University, 1108 Gengwen Road, Hangzhou, Zhejiang, 311231, China.
§ Present address: Eramet Ideas, 1 Avenue Albert Einstein, 78190 Trappes, France.

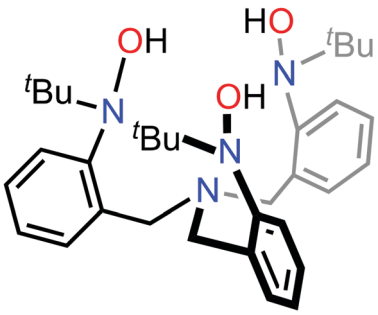

Fig. 1 Schematic structure of the H_3TriNOx ligand (L).

might reveal differences in anion–ligand binding. The gas-phase results indeed suggested a preference for association of H_3TriNOx with TcO_4^- over ReO_4^-.

Perrhenic acid, $HReO_4$, was first reported ~90 years ago,[11] pertechnic acid, $HTcO_4$, ~70 years ago,[12] and comparison of properties of the two was reported ~60 years ago.[13] For the current work, ESI studies revealed the gas-phase, bimetallic dimer of the two conjugate bases linked by a proton, $(TcO_4^-)(H^+)(ReO_4^-)$, which is a more fundamentally interesting and pertinent species than the initially pursued H_3TriNOx-containing complexes noted above. In the simple dimer, the two tetroxide anions are bound by a proton, with a net charge of −1 on the complex. This proton-bound dimer presented the opportunity to evaluate the relative proton affinities (PAs) of TcO_4^- and ReO_4^- using Cooks' kinetic method.[14–16] In addition to their proton bridge, some proton-bound dimers can exhibit secondary bonding interactions between the constituent anions, which can complicate interpretations in the context of relative PAs.[17] Accordingly, an important attribute of $(TcO_4^-)(H^+)(ReO_4^-)$ is that the structure and resulting bonding interaction can confidently be assigned as simple proton-bound dimer $[O_3Tc–O\cdots H\cdots O–ReO_3]^-$, such that its CID should indicate the relative PAs of TcO_4^- and ReO_4^-. Reported here is the result, based on CID of $(TcO_4^-)(H^+)(ReO_4^-)$, that the PA$[TcO_4^-]$ is greater than the PA$[ReO_4^-]$. Density functional theory (DFT) computations performed to understand this conclusion provided the anticipated relationship—PA$[TcO_4^-]$ > PA$[ReO_4^-]$—and showed that the difference is small, as expected for two such similar anions. Attempts to rationalize the relationship between these two PAs based on elementary molecular parameters suggest intertwined effects upon protonation that cannot be clearly resolved. Comparison of the gas-phase molecular properties with related solution properties such as basicities of TcO_4^- *versus* ReO_4^- reveals apparent correlations, but also provides caution against overreach of the significance of such correlations.

Experimental methods

Caution – The ^{99}Tc used in this work is radioactive and must be handled only with appropriate precautions in a suitable radiological laboratory.

Gas phase experiments were performed using an Agilent 6340 quadrupole ion trap mass spectrometer (QIT/MS) with an ESI source inside a radiological containment glovebox.[18] H_3TriNOx was synthesized as reported previously.[9] Anion complexes were produced by ESI of a solution containing ~100 μM of H_3TriNOx and ~500 μM of both $NH_4{}^{99}TcO_4$ and NH_4ReO_4 (isotopically natural Re) in ethanol (<10% water). Ions with a specific mass-to-charge ratio (m/z) are isolated and subjected to CID whereby they are resonantly excited and undergo energetic collisions with He, which ultimately leads to ion dissociation. CID products are identified by mass selective ion ejection from the QIT to a detector. Negative ion mass spectra were acquired using the following instrumental parameters: solution flow rate = 60 μL min^{-1}; nebulizer gas pressure = 15 psi; capillary voltage = +3500 V; end plate voltage offset = −500 V; dry gas flow rate = 5 L min^{-1}; dry gas temperature = 325 °C; capillary exit = −136.0 V; skimmer = −40.0 V; octopole 1 and 2 dc = −12.0 and −1.74 V; octopole RF amplitude = 200.0 V_{pp}; lens 1 and 2 = 5.0 and 60 V; trap drive = 74. Gas for ESI nebulization and drying in the ion transfer capillary was the boil off from liquid nitrogen. Results were obtained using nominal CID energies of ~0.2–0.6 V, with the specific value depending on ease of ion fragmentation. The CID voltage is an instrumental parameter that provides an indication of relative ion excitation, not actual ion energies.

Computational methods

Scalar relativistic Density Functional Theory (DFT) calculations were performed with the Gaussian 09[19] and ADF[20,21] software packages for the geometry optimizations and vibrational frequency analyses. The ground state geometries of all molecules were fully optimized in the gas phase without any symmetry constraints. Vibrational frequency analysis assured that the optimized structures are real minima on the potential energy surface. The calculated vibrational frequencies were obtained using the harmonic approximation. For the Gaussian calculations, scalar relativistic Stuttgart energy-consistent relativistic pseudopotentials and the associated ECP60MWB_ANO valence basis sets (SDD)[22] were used for the transition metal atoms. The split-valence double-ζ basis sets with polarization functions and diffusion functions on both heavy and hydrogen atoms (6-31++G**)[21,23] of Pople *et al.* were used for the remaining atoms (H, C, N and O). Except where otherwise notes, all calculations employed the B3LYP[24,25] hybrid functional, owing to its overall good performance for computing geometries of transition metal complexes. The basis set dependence of the energetics was studied with the 6-31G*, 6-311+G* and 6-31++G** basis sets, along with the same B3LYP functional. The natural atomic charges and bond orders were obtained by natural bond orbital (NBO) analysis utilizing the NBO6.0 code.[26,27]

To further understand the influence of relativistic effects on the gas-phase reaction energetics, geometry optimizations were performed with two different functionals (B3LYP and B3LYP-D3)[28] with the ADF code.[20] The scalar zeroth-order regular approximation (ZORA)[29] was used to model relativistic effects, in conjunction with

Slater type orbitals (STOs) of TZP quality (triple-zeta plus polarization functions).[30] Non-relativistic calculations were performed with similar basis sets. Geometry optimizations were performed without any symmetry constraints. Optimized geometries were always verified as minima on the potential energy surface by calculating the harmonic vibrational frequencies at the stationary point. The default convergence criterion of 10^{-6} a.u. and an integration parameter of 6.0 were applied.

Results and discussion

Electrospray ionization and collision induced dissociation

An ESI mass spectrum for a solution containing H_3TriNOx (denoted as L), TcO_4^- and ReO_4^- is shown in Fig. 2. Dominant species are complexes $(L)[(TcO_4^-)(H^+)(TcO_4^-)]$, $(L)[(TcO_4^-)(H^+)(ReO_4^-)]$ and $(L)[(ReO_4^-)(H^+)(ReO_4^-)]$, where the indicated constituent moieties, H_3TriNOx (L) and proton-bridged permetallate dimers, are based on results given below. Bare TcO_4^- and ReO_4^- are also significant ions in the ESI mass spectrum. Minor or negligible species include $(L)(TcO_4^-)$, $(L)(ReO_4^-)$, $(TcO_4^-)(H^+)(TcO_4^-)$, $(TcO_4^-)(H^+)(ReO_4^-)$ and $(ReO_4^-)(H^+)(ReO_4^-)$. There are apparently thermodynamic and/or kinetic factors that stabilize the three dominant larger coordination complex permetallate dimers relative to these smaller constituents, at least in gas phase. The ion abundances in the mass spectrum in Fig. 2 suggest preferential formation of gas-phase complexes comprising TcO_4^- over ReO_4^-. Considering that ReO_4^- abundances are distributed between two naturally occurring isotopes, ^{185}Re (37.4%) and ^{187}Re (62.6%), the net relative abundances of the complexes are: 1.00 $(L)[(TcO_4^-)(H^+)(TcO_4^-)]$: 0.90 $(L)[(TcO_4^-)(H^+)(ReO_4^-)]$; and 0.23 $(L)[(ReO_4^-)(H^+)(ReO_4^-)]$. The somewhat lower yield of the last of these suggests favored incorporation of TcO_4^- over ReO_4^-. It should be emphasized that this selectivity may not reflect solution speciation, but rather kinetic and/or energetic effects of ESI, which is a complex "solution-to-gas" process. Nevertheless, this apparent gas-phase separation factor is significantly greater than typically obtained for separating TcO_4^- from ReO_4^- in solution.[31] It should also be noted that a separation factor in solution of 1.00 : 0.23 at 300 K would correspond to a difference in complexation free energies of only $\sim$0.9 kcal mol^{-1} (*i.e.*, $\Delta G = -RT\ln K$).

To further probe the structure of $(L)[(TcO_4^-)(H^+)(ReO_4^-)]$ and the possibility of preferential binding of TcO_4^- over ReO_4^-, the complex was isolated and subjected to CID, with results shown in Fig. 3. The employed CID energy of only 0.20 V is qualitatively rather low when compared, for example, with 0.55 V required to fragment protonated H_4TriNOx$^+$ (HL^+, Fig. S1, ESI†). The dominant CID process apparent in Fig. 3 is neutral H_3TriNOx ligand loss to yield $(TcO_4^-)(H^+)(ReO_4^-)$. This principal pathway suggests a structure characterized by a H_3TriNOx ligand weakly bound to the bimetallic dimer, as we imply by the nomenclature $(L)[(TcO_4^-)(H^+)(ReO_4^-)]$. Also apparent in Fig. 3 is a small peak corresponding to ReO_4^-, which is also observed upon CID of $(TcO_4^-)(H^+)(ReO_4^-)$, as discussed below.

The appearance of the proton-bound dimer $(TcO_4^-)(H^+)(ReO_4^-)$ presented the opportunity to probe the relative PAs of TcO_4^- and ReO_4^- using Cooks' kinetic method.[14] For two generic bases B1 and B2 bound by a proton in dimer $(B1)(H^+)(B2)$, this simple approach reveals the base with the higher PA is that which preferentially retains the proton upon CID. The yield of dimer $(TcO_4^-)(H^+)(ReO_4^-)$ produced by CID of $(L)[(TcO_4^-)(H^+)(ReO_4^-)]$ was insufficient for secondary CID. Instead, the protonated bimetallic dimer was isolated from the parent ESI mass spectrum (Fig. 2 and Fig. S2, ESI†), with results for its CID shown in Fig. 4.

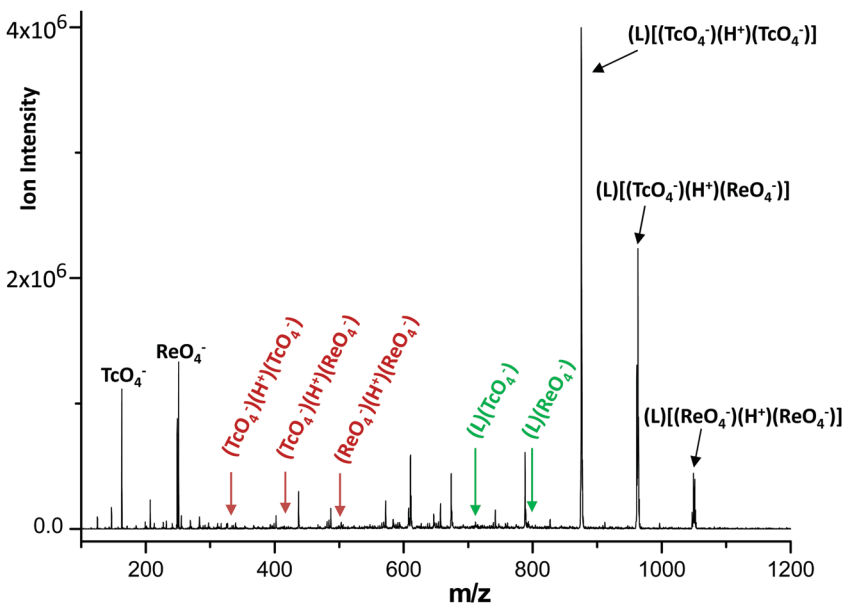

Fig. 2 ESI mass spectrum of solution of H_3TriNOx(L), NH_4TcO_4 and NH_4ReO_4 (concentration ratio 1 : 5 : 5). The *m*/*z* values of selected minor or minuscule products are as indicated by arrows and compositions in red (dimers) and green (monomers). Unassigned peaks may be due to ligand fragmentation as shown in ESI,† Fig. S1. Spectra with *y*-axis magnification to better reveal labelled low-intensity peaks are in ESI,† Fig. S2.

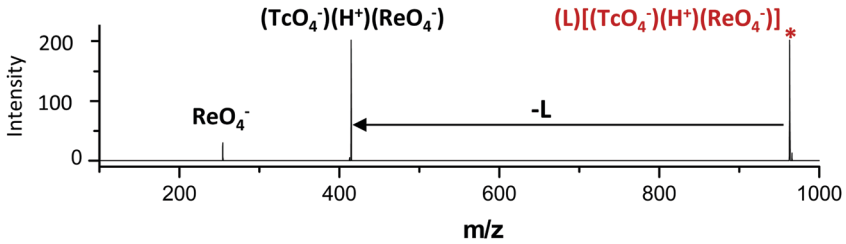

Fig. 3 CID mass spectrum of (L)[(TcO_4^-)(H^+)(ReO_4^-)] where L = H_3TriNOx. The nominal CID voltage was 0.20 V. The dominant CID pathway is loss of ligand L.

The two CID pathways for evaluating relative PAs of TcO_4^- and ReO_4^- are given by reactions (1) and (2). It is apparent from Fig. 4 that reaction (1) is dominant, with only minor (~1%) contribution from reaction (2). The CID energy used to fragment (TcO_4^-)(H^+)(ReO_4^-), 0.25 V, is only slightly higher than the 0.20 V to eliminate a ligand from (L)[(TcO_4^-)(H^+)(ReO_4^-)] (Fig. 3). The result that reaction (1) dominates over reaction (2) indicates that PA[TcO_4^-] > PA[ReO_4^-], where these PAs are defined as the enthalpies for dissociation reactions (3) and (4). Proton transfer reaction (5) is merely the difference between reactions (1) and (2), and also the difference between reactions (3) and (4). Some pertinent thermodynamics for these reactions are summarized by the following relationships: $\Delta H_3 \equiv$ PA[TcO_4^-]; $\Delta H_4 \equiv$ PA[ReO_4^-]; $\Delta H_5 = \Delta H_2 - \Delta H_1$ = PA[TcO_4^-] − PA[ReO_4^-]. The result that CID of [(TcO_4^-)(H^+)(ReO_4^-)] yields ReO_4^- *via* reaction (1) indicates that $\Delta H_2 > \Delta H_1$, $\Delta H_5 > 0$, and PA[TcO_4^-] > PA[ReO_4^-].

$$(TcO_4^-)(H^+)(ReO_4^-) \rightarrow HTcO_4 + ReO_4^- \quad (1)$$

$$(TcO_4^-)(H^+)(ReO_4^-) \rightarrow HReO_4 + TcO_4^- \quad (2)$$

$$HTcO_4 \rightarrow TcO_4^- + H^+ \quad (3)$$

$$HReO_4 \rightarrow ReO_4^- + H^+ \quad (4)$$

$$HTcO_4 + ReO_4^- \rightarrow HReO_4 + TcO_4^- \quad (5)$$

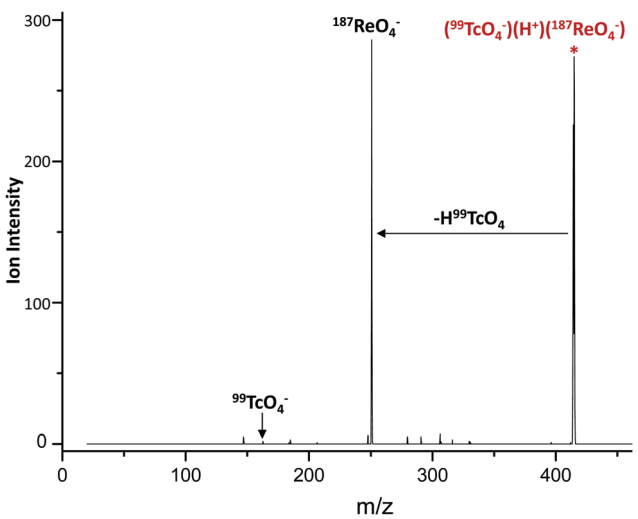

Fig. 4 CID mass spectrum of (TcO_4^-)(H^+)(ReO_4^-) at a nominal CID voltage of 0.25 V. The dominant CID anion product is ReO_4^- *via* reaction (1). The minor (<1%) yield of TcO_4^- is indicated.

Computed structures and energies of complexes

To understand the experimental observations, structures and energies of selected complexes were computed. The computed lowest energy structure of (L)[(TcO_4^-)(H^+)(ReO_4^-)] is shown in Fig. 5, with other low-energy structures shown in ESI.† The structure is characterized by two hydrogen bonds between hydroxyl groups of the ligand and the metal oxo moieties. Computed energies for selected dissociations of (L)[(TcO_4^-)(H^+)(ReO_4^-)] are summarized in Table 1. In accord with the CID results in Fig. 3, the lowest energy pathway is the observed ligand elimination reaction (6). Also apparent in the CID mass spectrum in Fig. 3 is a smaller peak assigned as ReO_4^-, which can be attributed to secondary dissociation *via* reaction (1) that was dominant for CID of (TcO_4^-)(H^+)(ReO_4^-). The structures here contrast with those previously reported for analogous species comprised of H_3TriNOx and halide anions.[10] The complex [L(HClBr)]$^-$, for example, is not a (Cl^-)(H^+)(Br^-) proton bound dimer coordinated by H_3TriNOx. Instead, it is essentially a protonated H_4TriNOx$^+$ coordinated by well-separated halide anions, Cl^- and Br^-. As a result, CID of [L(HClBr)]$^-$ does not result in neutral H_3TriNOx

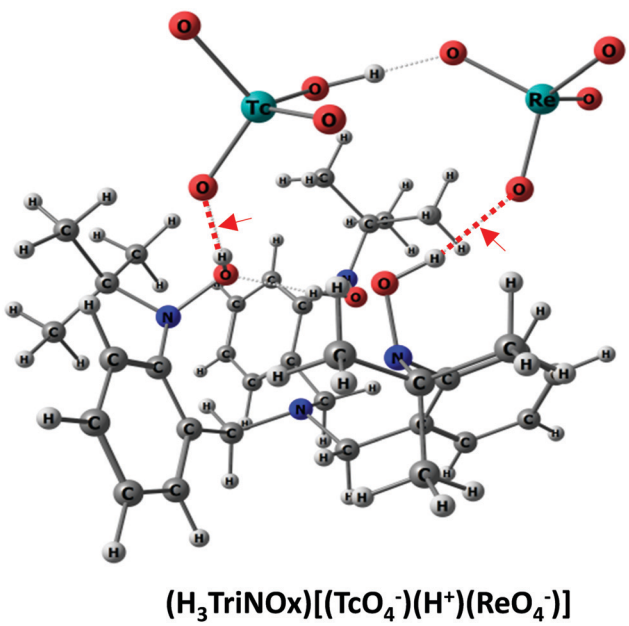

Fig. 5 Structure of [(H_3TriNOx)(TcO_4^-)(H^+)(ReO_4^-)] computed at the B3LYP/SDD/6-31G* level of theory. The two hydrogen bonds between metal oxo and ligand hydroxyl groups are indicated.

Table 1 Computed energies for different dissociations of (L)[(TcO_4^-)(H^+)-(ReO_4^-)] at the DFT/B3LYP/SDD/6-31G* level of theory (kcal mol^{-1}, zero point energy included)

Dissociation products	Energy
(L)(TcO_4^-) + $HReO_4$	ΔE = 17.23 ΔH = 16.89 ΔG = 7.44
(L)(ReO_4^-) + $HTcO_4$	ΔE = 14.42 ΔH = 14.08 ΔG = 4.86
(TcO_4^-)(H^+)(ReO_4^-) + L	ΔE = −16.84[a] ΔH = −17.18 ΔG = −30.14

[a] Using the 6-311+G* basis set, the computed ΔE is −0.17 kcal mol^{-1}.

ligand elimination in analogy to reaction (6), but rather HCl elimination to yield $[L(Br)]^-$. The different structures and behavior reflect that, in contrast to the bulky permetallate tetroxide anions, compact halide anions can form multiple hydrogen bonds to H_3TriNOx.

$$(L)[(TcO_4^-)(H^+)(ReO_4^-)] \rightarrow (TcO_4^-)(H^+)(ReO_4^-) + L \qquad (6)$$

The energy computed for reaction (6) using the 6-31G* basis set is substantially negative, ΔE_6 = −16.84 kcal mol^{-1}. This result suggests a net repulsive interaction between H_3TriNOx and (TcO_4^-)(H^+)(ReO_4^-), which would be remarkable given the hydrogen bonds—which are likely weak but presumably not repulsive—that are apparent in the structure shown in Fig. 5. However, the energy for reaction (6) using instead the 6-311+G* basis set is only very slightly negative, ΔE_6 = −0.17 kcal mol^{-1}. The 16.7 kcal mol^{-1} difference in the computed energy for reaction (6) using these two basis sets indicates substantial uncertainties in the energies in Table 1. Despite these uncertainties, the results in Table 1 show that the observed CID pathway is the lowest in energy, and the ligand is only weakly bound in (L)[(TcO_4^-)(H^+)(ReO_4^-)]. Given that quantifying ligand dissociation according to reaction (6) was not of primary interest, additional computations were not pursued to further refine the energy for this process.

The principal focus was instead on the simple observed CID process given by reaction (1), which dominated over alternative reaction (2). The computed energies for reactions (1) and (2) are summarized in Table 2, with the B3LYP/SDD/6-31++G** optimized structures of the involved species shown in Fig. 6. The computed structure of ReO_4^- is very similar to that previously reported by Wang and coworkers,[32] with the Re–O distance found here being only 0.01 Å longer. The rather low energies for reactions (1) and (2), ~30 kcal mol^{-1}, are consistent with the low CID voltage needed to drive the reaction. In contrast to the 16.6 kcal mol^{-1} change in the energy for reaction (5) upon switching from basis set 6-31G* to 6-311+G*, the variations in computed energies for reactions (1) and (2) were much smaller for all the Gaussian basis sets employed (6-31G*, 6-311+G* and 6-31++G**). To further understand the influence of relativistic effects on the gas-phase reaction energetics of reactions (1) and (2),

Table 2 Computed energies for dissociation of [(TcO_4^-)(H^+)(ReO_4^-)][a]

Reaction[b]	Energy	SDD/ 6-31G*[c]	SDD/ 6-311+G*[c]	SDD/ 6-31++G**[c]	ZORA-B3LYP[d]	ZORA-B3LYP-D3[d]
(1)	ΔE	28.71	27.40	28.07	24.99	25.82
	ΔH	28.35	27.05	27.81	24.93	25.91
	ΔG	21.24	21.91	19.85	15.96	16.56
(2)	ΔE	31.84	29.99	30.92	28.12	28.95
	ΔH	31.47	29.66	30.66	28.07	29.05
	ΔG	25.04	25.13	22.70	19.09	19.69
ΔH_5[e]	ΔE	3.13	2.59	2.85	3.13	3.13
	ΔH	3.12	2.61	2.85	3.14	3.14
	ΔG	3.80	3.22	2.85	3.13	3.13

[a] Energies in kcal mol^{-1} at 298.15 K. Zero point energy is included. [b] Reaction (1) products are $HTcO_4$ + ReO_4^-; reaction (2) products are $HReO_4$ + TcO_4^-. [c] Using Gaussian09 DFT/B3LYP with the indicated basis set and ECP. [d] Using the ADF code (scalar ZORA) with the indicated functional and ZORA-TZP basis sets. [e] Difference between the energies for (2) and (1).

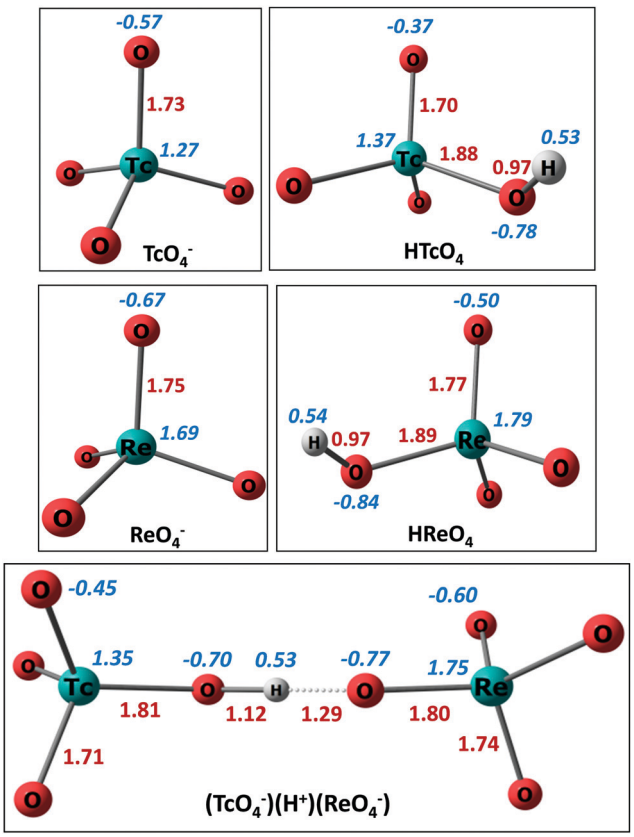

Fig. 6 Structures of the species in reactions (1) and (2) optimized at the B3LYP/SDD/6-31++G** level of theory. Selected bond distances (Å) are in red; NPA atomic charges are in blue italics.

frozen core scalar ZORA calculations have been performed with two different functionals (B3LYP and B3LYP-D3) with the ADF code (ZORA-TZP basis sets). The resulting energies in Table 2 reveal that reaction (1) is thermodynamically favored over reaction (2), which is consistent with the Gaussian ECP results. Most significantly, the computations indicate that reaction (1) is lower

in energy than reaction (2), by ~3 kcal mol^{-1} at all the considered levels of theory. The computations thus concur with the observation that CID reaction (1) is dominant, and the resulting interpretation that PA[TcO_4^-] > PA[ReO_4^-]. The absolute PAs computed using B3LYP/SDD/6-31++G** are PA[TcO_4^-] = 300.07 kcal mol^{-1} and PA[ReO_4^-] = 297.23 kcal mol^{-1}, which yield a difference of 2.84 kcal mol^{-1} that corresponds to ΔH_5 in Table 2. To further assess different functionals, absolute PAs were computed at the ZORA/TZP level with DFT functionals B3LYP, B3LYP-D3, PBE0, PBE, M06-2X, and CAM-B3LYP (ESI,† Table S4) using ADF code. For each functional PA[TcO_4^-] is greater than PA[ReO_4^-], with the difference ranging from 2.96 kcal mol^{-1} for PBE to 4.55 kcal mol^{-1} for CAM-B3LYP. Similarly, using different basis sets B3LYP/TZP and B3LYP/TZ2P the calculated PA[TcO_4^-] is greater than PA[ReO_4^-], by 3.13 kcal mol^{-1} and 2.82 kcal mol^{-1}, respectively (ESI,† Table S5). Although the disparity between the PAs is small—*ca.* 1% of their absolute values of ~300 kcal mol^{-1}—the slightly higher PA[TcO_4^-] is clearly manifested in CID (Fig. 4).

Assessment of bonding and proton affinities of TcO_4^- and ReO_4^-

To understand the origins of the relative PAs of TcO_4^- and ReO_4^- we consider the structures and bond parameters for the species shown in Fig. 6. Some pertinent parameters are shown in Fig. 6 and Table 3, with additional values in ESI.† The NPA charges indicate significantly more negative charges on the O atoms in ReO_4^- ($\delta = -0.67$) *versus* TcO_4^- ($\delta = -0.57$), a result in accord with previous computational assessments.[31,33] A resulting straightforward prediction from more negative charges on the O atoms of ReO_4^- *versus* TcO_4^- is that PA[ReO_4^-] should be greater than PA[TcO_4^-], which contrasts with the experimental and computational results.

A complete assessment must consider charges on all O atoms before and after protonation. The charge on the protonated O is −0.84 in $HReO_4$ and −0.78 in $HTcO_4$, suggesting again that PA[ReO_4^-] should be greater than PA[TcO_4^-]. The charges on the other three O atoms are also more negative for $HReO_4$ (−0.50) *versus* $HTcO_4$ (−0.37). Upon protonation, for both the Re and Tc species the charge on the added H is ~0.53, the total charge on the four O atoms becomes less negative by 0.37, and the charge on the metal center becomes more positive by 0.10. Despite these similarities, a notable difference between the two systems is a slightly different charge redistribution upon protonation, with a result that the charge on the protonated O becomes more negative by −0.17 for $HReO_4$, while by −0.21 for $HTcO_4$. This polarization difference is insufficient to render the O charge more negative in the latter, such that there remains an apparent inconsistency between the relative PAs and O atom charges.

A key underlying consideration for understanding the apparent inconsistency between O atom charges and PA is that PA, like any reaction energy, is a function of all changes in bonding between reactants and products. Thus, PA not only reflects the attractive interaction between H^+ and the $O^{-\delta}$ in metal oxo MO_4^-; it also reflects changes in charges and bonds in the MO_4^- moiety that result from perturbations introduced by proton association. The NPA charges in Fig. 6 indicate that the bonds in both ReO_4^- and $HReO_4$ are significantly more polar—*i.e.* more ionic and less covalent—than the corresponding bonds in TcO_4^- and $HTcO_4$. Although the bonding is not quantified here, it is reasonable that the changes in charge distribution due to protonation should more substantially disrupt the more ionic bonds in ReO_4^- *versus* those in more covalent TcO_4^-. Such disruption that results in bond weakening should disfavor protonation and diminish the relative PA of ReO_4^-. It should be emphasized that the difference between PA[TcO_4^-] and PA[ReO_4^-] is minor relative to the overall metal–oxo bonding that is perturbed upon protonation. A key point is that relative PAs of inorganic species like these cannot necessarily be predicted from elementary molecular parameters such as effective atomic charges; the holism of perturbations needs to be considered.

From the parameters in Fig. 6 for (TcO_4^-)(H^+)(ReO_4^-) it is evident that the higher PA for TcO_4^- *versus* ReO_4^- is clearly revealed in the structure of the protonated dimer. In accord with ultimate dissociation to $HTcO_4$ and ReO_4^-, the O_3TcO–H distance (1.12 Å) in the dimer is significantly shorter than the O_3ReO–H distance (1.29 Å). In lieu of the simplified representation as (TcO_4^-)(H^+)(ReO_4^-), the following actual computed charges on the three moieties in the complex are obtained from the constituent atomic charges (Table S2, ESI†): ($TcO_4^{-0.715}$)-($H^{+0.533}$)($ReO_4^{-0.815}$). Although such charge assignments are not physically observable quantities, they do indicate relative charge distributions. In view of the less negative O atom charges in bare TcO_4^- *versus* ReO_4^-, it is tempting to attribute the greater PA[TcO_4^-] *versus* PA[ReO_4^-] to the greater polarizability of Tc (79 a.u.) and TcO_4^- (computed here as 57.3 a.u.) relative to Re (62 a.u.) and ReO_4^- (computed as 56.3 a.u.).[34] However, as noted above, after proton association the charge on $O^{-\delta}$ in the hydroxyl group in $HTcO_4$ ($\delta = 0.78$) remains less negative than that in $HReO_4$ ($\delta = 0.84$). In accord with the higher polarizability of TcO_4^-, the enhancement in negative charge on the protonated O atom is greater for the conversion of TcO_4^--to-$HTcO_4$ ($\Delta\delta = 0.21$) than for ReO_4^--to-$HReO_4$ ($\Delta\delta = 0.17$). However, the difference in polarization upon protonation is insufficient to yield a more negative oxygen charge in $HTcO_4$ *versus* $HReO_4$. Neither the oxygen charges in the bare MO_4^- nor those in the protonated HMO_4 account for the relative PAs.

Table 3 Selected bond distances (Å), NBO bond orders, and stretching frequencies (cm^{-1}) at the B3LYP/SDD/6-31++G* level of theory

		TcO_4^-	$HTcO_4$	ReO_4^-	$HReO_4$	(TcO_4^-)(H^+)(ReO_4^-)[a]
M–O	Distance	1.733	1.696	1.754	1.719	1.708/1.738
	NBO	1.60	1.79	1.58	1.77	1.71/1.66
	Frequency	915	986	943	965	976/967
M–OH	Distance	—	1.882	—	1.891	1.806/1.796
	NBO	—	0.91	—	0.91	1.16/1.27
	Frequency		692		684	881/743
MO–H	Distance	—	0.971	—	0.970	1.117/1.291
	NBO	—	0.71	—	0.70	0.43/0.27

[a] Parameters are expressed as "M = Tc/M = Re".

As remarked above, not only the $O^{-\delta}\cdots H$ bonds, but additionally the perturbations to all bonds in conversion of MO_4^- to HMO_4 need to be considered to effectively assess and predict PAs.

To the extent that relativistic effects influence the PAs of the MO_4^- species, the consequences should be greater for M = Re with nuclear charge $Z = 75$, *versus* M = Tc with $Z = 43$. Using the ADF code and the B3LYP hybrid functional yields non-relativistic PA[TcO_4^-] = 307.77 kcal mol^{-1} and PA[ReO_4^-] = 306.45 kcal mol^{-1}. These values are *ca.* 7 kcal mol^{-1} for Tc and 9 kcal mol^{-1} for Re higher than those obtained using Gaussian with the same functional and scalar relativistic ECPs. Applying a relativistic correction using ZORA with ADF yields PA[TcO_4^-] = 306.75 kcal mol^{-1} and PA[ReO_4^-] = 303.62 kcal mol^{-1}. The relativistic correction to the ADF ReO_4^- value, ΔPA = 2.83 kcal mol^{-1}, is indeed greater than that for TcO_4^-, ΔPA = 1.02 kcal mol^{-1}. The ADF results suggest that without the reality of relativistic effects, the PAs of TcO_4^- and ReO_4^- would be even more similar. Notably, the PA ordering remains the same for the relativistic and non-relativistic ADF values, PA[TcO_4^-] > PA[ReO_4^-], and the difference between the relativistic ADF values, 3.13 kcal mol^{-1}, is close to the difference of 2.84 kcal mol^{-1} using Gaussian and ECPs.

Gould and Miller determined thermodynamics of rhenium species formed in flames.[35] Of particular relevance to the present study is the following studied reaction: $e^- + HReO_4 \rightarrow ReO_4^- + H$. The enthalpy change for this reaction, 4 $\pm$ 12 kcal mol^{-1}, combined with IE[$H \rightarrow H^+ + e^-$] = 313.59 kcal mol^{-1},[36] yields PA[ReO_4^-] = 318 $\pm$ 12 kcal mol^{-1}. All three PA[ReO_4^-] values computed here, particularly the relativistic ZORA value of 303.62 kcal mol^{-1}, are in reasonable accord with the experimental value.

Relationship between gas and solution chemistry

As noted above, CID of $(TcO_4^-)(H^+)(ReO_4^-)$ essentially probes whether the enthalpy of proton transfer reaction (5), ΔH_5, is positive or negative, to preferentially yield ReO_4^- or TcO_4^-, respectively. The experimental result that CID yields mostly ReO_4^- indicates that $\Delta H_5 > 0$. The B3LYP/SDD/6-31++G** computations properly provide a positive value for the enthalpy ΔH_5, 2.85 kcal mol^{-1}, which is coincidentally identical to the free energy ΔG_5 computed at this level of theory (Table 2). The aqueous solution reaction corresponding to gas-phase reaction (5) is reaction (7). Proton association constants obtained for TcO_4^- and ReO_4^- in aqueous solution under identical conditions provide an equilibrium constant for reaction (7) of $K_7 = 0.49$ at 298 K,[37] which corresponds to $\Delta G_7 = 0.43$ kcal mol^{-1}.

$$HTcO_4(aq) + ReO_4^-(aq) \rightarrow HReO_4(aq) + TcO_4^-(aq) \qquad (7)$$

The experimental result that the solution basicity of TcO_4^- is greater than that of ReO_4^- is in qualitative accord with the higher gas-phase PA of TcO_4^- *versus* ReO_4^-. However, even this qualitative accord is quite possibly fortuitous given the very different nature of gas-phase PA and solution basicity. Whereas gas-phase PA depends only on the binding energy to a proton, solution basicity reflects additionally the multifarious bonding transformations due to changes in solvation. In essence, the energy associated with the ensemble of ion–solution interactions cannot be simplified to consideration of only the anion–receptor interactions,[38] including when the "receptor" is a proton. Furthermore, whereas gas-phase PA probes the enthalpy of proton association, solution basicity reflects the free energy of association in which entropy effects are typically substantial.[38]

Despite the need for discretion when inferring solution properties from those of constituent unsolvated gas-phase species, it is appealing—and reasonable—to cautiously employ simple molecular properties to rationalize, understand, and predict more complex condensed phase phenomena. The rather disparate charge distributions computed for TcO_4^- and ReO_4^- (Fig. 6) are a case in point. The more energetically favorable hydration, and less effective extraction, of ReO_4^- *versus* TcO_4^- may reflect the generally greater "hydrophilicity" of ReO_4^-,[31] which can in turn be attributed to its more polar nature. It is additionally tempting to partly attribute the higher acidity of $HReO_4$ *versus* $HTcO_4$ to enhanced hydration of more polar ReO_4^- *versus* TcO_4^-, an effect that should preferentially favor dissociation of $HReO_4$. However, this oversimplified assessment neglects differences between hydration of the undissociated acids. Specifically, the greater $M–O^{-\delta}$ bond polarity in $HReO_4$ ($\delta = 0.57$) *versus* $HTcO_4$ ($\delta = 0.37$) should preferentially enhance hydration of $HReO_4$, and thus suppress its dissociation and acidity relative to $HTcO_4$. The result that computed molecular properties like atomic charges can be employed to rationalize contradictory effects illustrates the need for caution in inferring solution behavior from selected properties of isolated gas-phase species.

Conclusions

Gas-phase protonated dimer $(TcO_4^-)(H^+)(ReO_4^-)$ was produced by ESI in sufficient abundance for isolation and dissociation by CID. The dominant dissociation pathway to $HTcO_4$ and ReO_4^- reveals that PA[TcO_4^-] is greater than PA[ReO_4^-]. Energies computed by DFT are in accord with this comparison, with the computed PAs differing by only $\sim$1% ($\sim$3 kcal mol^{-1}) relative to their absolute values ($\sim$300 kcal mol^{-1}). Consideration of computed molecular properties indicates that the higher PA[TcO_4^-] *versus* PA[ReO_4^-] cannot be rationalized from differences in negative charges on the proton-receptor O atoms, which are more negative in the Re species. Instead, the entirety of bond formation and disruption needs to be considered to understand the results; the lower PA[ReO_4^-] *versus* PA[TcO_4^-] suggests greater disruption of more ionic Re–O bonds upon protonation. Although the relative PAs are in qualitative agreement with reports that TcO_4^- is a stronger aqueous base than ReO_4^-, restraint is advisable when inferring insights into complex condensed phase phenomena from simple gas-phase molecular properties.

Evaluating relative PAs of metal anion dimer complexes is a potential means to assess charge distributions and bonding in constituent bare and protonated species. It is anticipated that other such anions may present more substantial PA differences than do chemically very similar TcO_4^- and ReO_4^-. Generation by

ESI of the dimer $(TcO_4^-)(H^+)(ReO_4^-)$ with a binding energy of only $\sim$30 kcal mol^{-1} suggests that it should be feasible to prepare other such proton bound dimers. An extension of the present type of study would be CID of dimers containing actinide tetroxide anions like NpO_4^- and PuO_4^-.[39,40] Dimer $(NpO_4^-)(H^+)(PuO_4^-)$ should have a simple proton-bridged structure, $[O_3Np{-}O\cdots H\cdots OPuO_3]^-$, CID of which would reveal the relative magnitudes of PA$[NpO_4^-]$ *versus* PA$[PuO_4^-]$. These relative PAs should reflect bonding differences between Np–O and Pu–O bonds, and their perturbations upon protonation.

Conflicts of interest

There are no conflicts to declare.

Acknowledgements

This work was supported primarily by the Center for Actinide Science and Technology, an Energy Frontier Research Center funded by the U.S. Department of Energy, Office of Science, Basic Energy Sciences (DOE BES) under Award Number DE-SC0016568. WWL was supported by the DOE BES Heavy Element Chemistry Program at Lawrence Berkeley National Laboratory under Contract DE-AC02-05CH11231.

References

1 G. R. Choppin, Inner versus outer sphere complexation of f-elements, *J. Alloys Compd.*, 1997, **249**, 9–13.
2 C. D. Williams and P. Carbone, A classical force field for tetrahedral oxyanions developed using hydration properties: The examples of pertechnetate (TcO_4^-) and sulfate (SO_4^{2-}), *J. Chem. Phys.*, 2015, **143**, 174502.
3 F. R. Chen, P. C. Burns and R. C. Ewing, Near-field behavior of Tc-99 during the oxidative alteration of spent nuclear fuel, *J. Nucl. Mater.*, 2000, **278**, 225–232.
4 E. Dadachova, B. Bouzhzah, L. S. Zuckier and R. G. Pestell, Rhenium-188 as an alternative to iodine-131 for treatment of breast tumors expressing the sodium/iodide symporter (NIS), *Nucl. Med. Biol.*, 2002, **29**, 13–18.
5 D. W. Zhang, T. K. Ronson, J. Mosquera, A. Martinez and J. R. Nitschke, Selective Anion Extraction and Recovery Using a $Fe^{II}_4L_4$ Cage, *Angew. Chem., Int. Ed.*, 2018, **57**, 3717–3721.
6 A. Ravi, A. S. Oshchepkov, K. E. German, G. A. Kirakosyan, A. V. Safonov, V. N. Khrustalev and E. A. Kataev, Finding a receptor design for selective recognition of perrhenate and pertechnetate: hydrogen vs. halogen bonding, *Chem. Commun.*, 2018, **54**, 4826–4829.
7 R. Alberto, G. Bergamaschi, H. Braband, T. Fox and V. Amendola, (TcO_4)-Tc-99-: Selective Recognition and Trapping in Aqueous Solution, *Angew. Chem., Int. Ed.*, 2012, **51**, 9772–9776.
8 L. Mei, F. Z. Li, J. H. Lan, C. Z. Wang, C. Xu, H. Deng, Q. Y. Wu, K. Q. Hu, L. Wang, Z. F. Chai, J. Chen, J. K. Gibson and W. Q. Shi, Anion-adaptive crystalline cationic material for $^{99}TcO_4^-$ trapping, *Nat. Commun.*, 2019, 10.
9 J. A. Bogart, C. A. Lippincott, P. J. Carroll and E. J. Schelter, An Operationally Simple Method for Separating the Rare-Earth Elements Neodymium and Dysprosium, *Angew. Chem., Int. Ed.*, 2015, **54**, 8222–8225.
10 T. Cheisson, J. W. Jian, J. Su, T. M. Eaton, M. R. Gau, P. J. Carroll, E. R. Batista, P. Yang, J. K. Gibson and E. J. Schelter, Halide anion discrimination by a tripodal hydroxylamine ligand in gas and condensed phases, *Phys. Chem. Chem. Phys.*, 2019, **21**, 19868–19878.
11 J. T. Dobbins and J. K. Colehour, The preparation of perrhenic acid, *J. Am. Chem. Soc.*, 1934, **56**, 2054.
12 J. W. Cobble, W. T. Smith and G. E. Boyd, Thermodynamic Properties of Technetium and Thenium Compounds. 2. Heats of Formation of Technetium Heptoxide and Pertechnic Acid, Potential of the Technetium(IV)-Technetium(VII) Couple, and a Potential Diagram for Technetium, *J. Am. Chem. Soc.*, 1953, **75**, 5777–5782.
13 C. L. Rulfs, R. A. Pacer and R. F. Hirsch, Pertechnic Acid – an Aperiodic Variation in Acid Strength, *Nature*, 1963, **199**, 66.
14 S. A. Mcluckey, D. Cameron and R. G. Cooks, Proton Affinities from Dissociations of Proton-Bound Dimers, *J. Am. Chem. Soc.*, 1981, **103**, 1313–1317.
15 P. B. Armentrout, Special feature: Commentary – Is the kinetic method a thermodynamic method?, *J. Mass Spectrom.*, 1999, **34**, 74–78.
16 R. G. Cooks, J. S. Patrick, T. Kotiaho and S. A. Mcluckey, Thermochemical Determinations by the Kinetic Method, *Mass Spectrom. Rev.*, 1994, **13**, 287–339.
17 G. L. Hou, X. B. Wang and M. Valiev, Formation of $(HCOO^-)(H_2SO_4)$ Anion Clusters: Violation of Gas-Phase Acidity Predictions, *J. Am. Chem. Soc.*, 2017, **139**, 11321–11324.
18 D. Rios, P. X. Rutkowski, D. K. Shuh, T. H. Bray, J. K. Gibson and M. J. Van Stipdonk, Electron transfer dissociation of dipositive uranyl and plutonyl coordination complexes, *J. Mass Spectrom.*, 2011, **46**, 1247–1254.
19 M. Frish, *et al.*, *Gaussian 09 Revision C.01*, 2010.
20 E. Baerends, *et al.*, *ADF 2017*, SCM, Vrije Universiteit, Amsterdam, 2017.
21 G. te Velde, F. M. Bickelhaupt, E. J. Baerends, C. F. Guerra, S. J. A. Van Gisbergen, J. G. Snijders and T. Ziegler, Chemistry with ADF, *J. Comput. Chem.*, 2001, **22**, 931–967.
22 X. Y. Cao, M. Dolg and H. Stoll, Valence basis sets for relativistic energy-consistent small-core actinide pseudopotentials, *J. Chem. Phys.*, 2003, **118**, 487–496.
23 R. Krishnan, J. S. Binkley, R. Seeger and J. A. Pople, Self-Consistent Molecular-Orbital Methods. 20. Basis Set for Correlated Wave-Functions, *J. Chem. Phys.*, 1980, **72**, 650–654.
24 A. D. Becke, Density-Functional Thermochemistry. 3. The Role of Exact Exchange, *J. Chem. Phys.*, 1993, **98**, 5648–5652.
25 C. T. Lee, W. T. Yang and R. G. Parr, Development of the Colle-Salvetti Correlation-Energy Formula into a Functional of the Electron-Density, *Phys. Rev. B: Condens. Matter Mater. Phys.*, 1988, **37**, 785–789.
26 A. E. Reed, L. A. Curtiss and F. Weinhold, Intermolecular Interactions from a Natural Bond Orbital, Donor-Acceptor Viewpoint, *Chem. Rev.*, 1988, **88**, 899–926.

27 E. D. Glendening, J. K. Badenhoop, A. E. Reed, J. E. Carpenter, J. A. Bohmann, C. M. Morales and F. Weinhold, *NBO 6.0*, University of Wisconsin, Madison, WI, 2017.

28 S. Grimme, J. Antony, S. Ehrlich and H. Krieg, A consistent and accurate ab initio parametrization of density functional dispersion correction (DFT-D) for the 94 elements H-Pu, *J. Chem. Phys.*, 2010, **132**, 154104.

29 E. van Lenthe, E. J. Baerends and J. G. Snijders, Relativistic Regular Two-Component Hamiltonians, *J. Chem. Phys.*, 1993, **99**, 4597–4610.

30 E. van Lenthe and E. J. Baerends, Optimized Slater-type basis sets for the elements 1-118, *J. Comput. Chem.*, 2003, **24**, 1142–1156.

31 E. A. Katayev, N. V. Boev, V. N. Khrustalev, Y. A. Ustynyuk, I. G. Tananaev and J. L. Sessler, Bipyrrole- and dipyrromethane-based amido-imine hybrid macrocycles. New receptors for oxoanions, *J. Org. Chem.*, 2007, **72**, 2886–2896.

32 W. J. Chen, H. J. Zhai, X. Huang and L. S. Wang, On the electronic structure of mono-rhenium oxide clusters: ReOn- and ReOn (n = 3, 4), *Chem. Phys. Lett.*, 2011, **512**, 49–53.

33 A. J. Bridgeman and G. Cavigliasso, Density-functional investigation of bonding in tetrahedral MO_4 anions, *Polyhedron*, 2001, **20**, 2269–2277.

34 P. Schwerdtfeger and K. J. Nagle, Table of Static Dipole Polarizabilities of the Neutral Elements in the Periodic Table (vol 117, pg 1200, 2018), *Mol. Phys.*, 2019, **117**, 1585.

35 R. K. Gould and W. J. Miller, Electron Attachment and Compound Formation in Flames. 6. Negative-Ion and Compound Formation in Flames Containing Rhenium and Potassium, *J. Chem. Phys.*, 1975, **62**, 644–649.

36 S. G. Lias, H. M. Rosenstock, K. Draxl, B. W. Steiner, J. T. Herron, J. L. Jolmes, R. D. Levin, J. F. Liebman and S. A. Kafafi, NIST Chemistry WebBook, NIST Standard Reference Database Number 69, National Institute of Standards and Technology, Gaithersburg, MD, 2018.

37 T. Nakashima and K. H. Lieser, Proton Association of Pertechnetate, Perrhenate and Perchlorate Anions, *Radiochim. Acta*, 1985, **38**, 203–206.

38 F. P. Schmidtchen, Hosting anions. The energetic perspective, *Chem. Soc. Rev.*, 2010, **39**, 3916–3935.

39 J. K. Gibson, W. A. de Jong, P. D. Dau and Y. Gong, Heptavalent Actinide Tetroxides NpO4- and PuO4-: Oxidation of Pu(V) to Pu(VII) by Adding an Electron to PuO4, *J. Phys. Chem. A*, 2017, **121**, 9156–9162.

40 J. E. C. Wren and G. Schreckenbach, Neptunium(VII) in high-ionic-strength alkaline solutions – $[NpO_2(OH)_4]^{1-}$ or $[NpO_4(OH)_2]^{3-}$?, *Can. J. Chem.*, 2009, **87**, 1436–1443.